Newcastle University ePrints

Marin I, Turta C, Benniston AC, Harrington RW, Clegg W. Homoleptic and Heteroleptic Ruthenium(II) Complexes based on 2,6-bis(quinolin-2-yl)pyridine Ligands: Multiple Charged State Modules for Potential Density Memory Storage. *European Journal of Inorganic Chemistry* 2015.

DOI: http://dx.doi.org/10.1002/ejic.201403088

Homoleptic and Heteroleptic Ruthenium(II) Complexes based on 2,6-bis(quinolin-2-yl)pyridine Ligands: Multiple Charged State Modules for Potential Density Memory Storage

Ion Marin,[a] Constantin Turta,[a] Andrew C. Benniston,*[b] Ross W. Harrington[c] and William Clegg[c]

Abstract: The two ligands 2,6-bis(4-methylquinolin-2-yl)pyridine (**L_1**) and diethyl 2,2′-(pyridine-2,6-diyl)bis(quinolone-4-carboxylate) (**L_2**) were used to prepare the homoleptic $[Ru(\mathbf{L_2})_2](PF_6)_2$ (**RU1**) and heteroleptic $[Ru(\mathbf{L_1})(\mathbf{L_2})](PF_6)_2$ (**RU2**) complexes. DFT calculations (B3PW91, 3-21G**) performed on both **RU1** and **RU2** revealed that redox at the ruthenium site for **RU2** is less positive by around 110 mV. The corollary is that one-electron ligand-based reduction for **RU2** is more cathodic by 80 mV. Electrochemistry experiments confirmed that the prediction is qualitatively correct and that the complexes can each hold up to five electrons reversibly.

Introduction

Polypyridyl ligands [e.g. 2,2′-bipyridine (bipy), 2,2′:6′,2″-terpyridine (terpy)] and their complexes with metal ions such as ruthenium(II), osmium(II) and iridium(III) hold an especially prominent place in the development side of photoactive and redox-active supramolecular systems.[1] In distinctive cases the metal complex is the focal photoactive segment to instigate cascade energy and electron transfer processes, and in other situations it is the essential “glue” to hold together large arrays.[2] By precise choice of metal and ligands the redox behavior is manipulated to facilitate charge migration in unique directions.[3] The past three decades have witnessed great efforts to design new ligands, especially those which are tridentate, to circumvent the poor photochemistry observed for $[Ru(terpy)_2]^{2+}$ complexes.[4] It is recognized that the poor bite angle for the terpy ligands in $[Ru(terpy)_2]^{2+}$ means that the e_g* orbitals are close in energy to the occupied π* ligand orbital of the triplet metal-to-ligand charge transfer state (^{3}MLCT).[5] As a consequence thermally activated depopulation of the ^{3}MLCT state is highly efficient and the luminescence lifetime is sub-ns. Modification of the basic terpyridine structure has certainly been extremely popular and the exchange of the two outer pyridines for quinolone groups has produced the most dramatic and contrasting results. Early work concentrated on 2,6-di(quinolin-2-yl)pyridine, **DQ2P** (Figure 1), and its ruthenium(II) complex which showed no improvement in excited state lifetime performance at room temperature.[6] In complete contrast the later reported ruthenium(II) complex of the ligand 2,6-di(quinolin-8yl)pyridine, **DQ8P** (Figure 1), is highly luminescent and the excited state lifetime is several microseconds.[7] Considering the failure of **DQ2P** and its analogues to improve the photophysical properties of transition metal ion complexes, not surprisingly the ligands have received less attention. However, one slightly overlooked and notable feature of bis-**DQ2P** ruthenium(II) complexes is their electrochemistry, and in particular the reduction portion of cyclic voltammograms.[8] Four closely spaced reversible waves were reported, essentially meaning that complexes are not only proficient at multi-electron storage but may be applicable to high density memory storage.[9] Here the concept is to access multiple-charged states at distinct voltages reversibly; the ferrocene molecule is a prime example consisting of two states: the neutral and the mono-positive (ferrocenium) state.[10] In contrast, a bis-**DQ2P** ruthenium(II) complex would be considered a five-state system, starting neutral and adding in sequentially four electrons. However, when re-examining the electrochemistry for two derivatives of **DQ2P** we noticed that upon reduction at least one more redox state is readily accessible. An interesting conundrum arises because of this observation; namely, where does the fifth electron reside, considering that tri-anion formation is necessary if the final electron addition is solely ligand-based?[11]

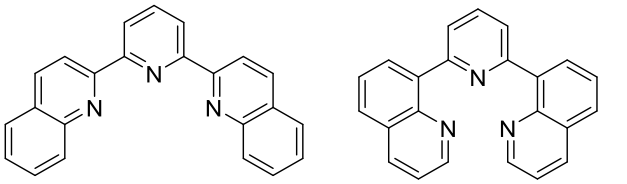

2,6-di(quinolin-2-yl)pyridine **DQ2P**

2,6-di(quinolin-8-yl)pyridine **DQ8P**

Figure 1. Examples of quinolone-based tridentate ligands, showing the subtle difference in chelate ring arrangement by alteration in N-atom positions. Note: the drawings to do not represent the energy-minimized conformations but those required for tridentate ligation.

[a] Mr I. Marin, Prof. C. Turta
Institute of Chemistry
Academy of Sciences of Moldova
3, Academiei str., Chisinau, Republic of Moldova, MD-2028.
[b] Prof. A. C. Benniston
Molecular Photonics Laboratory, School of Chemistry
Newcastle University
Newcastle upon Tyne, NE1 7RU, UK
E-mail: a.c.benniston@ncl.ac.uk
[c] Dr R. W. Harrington, Prof W. Clegg
Crystallography Laboratory
School of Chemistry
Newcastle University
Newcastle upon Tyne, NE1 7RU, UK

Supporting information for this article is given via a link at the end of the document.

Results and Discussion

Synthesis

Prior work has shown that ligands based on the **DQ2P** unit are prepared by applying a one-pot Pfitzinger reaction.[12] Therefore, using established procedures the two ligands $\mathbf{L_1}$ and $\mathbf{L_2}$ were synthesized by this method and fully characterized. Crystal structures for both ligands (see Supporting Information) confirm the *anti-anti* arrangement of the nitrogen atoms. Our interest was to prepare both homoleptic and heteroleptic ruthenium(II) complexes based on these two ligands, and so the first step was to prepare a mono-ligand ruthenium(III) synthon. Thus, reaction of $\mathbf{L_2}$ with $RuCl_3$ proceeded smoothly to produce the adduct $\mathbf{RuL_2}$ as a dark green solid in 79% yield. A very strong band at 1715 cm^{-1} in the IR spectrum confirmed that the ethyl ester remained intact during complexation. To facilitate attachment of a second ligand to $\mathbf{RuL_2}$ the chloro ligands were removed by reaction with $AgBF_4$, changing the color of the solution from green to purple. The *in-situ* generated solvated complex was reacted under reflux in *n*-BuOH with either $\mathbf{L_1}$ or $\mathbf{L_2}$ to produce the heteroleptic complex **RU2** or homoleptic complex **RU1**, respectively.

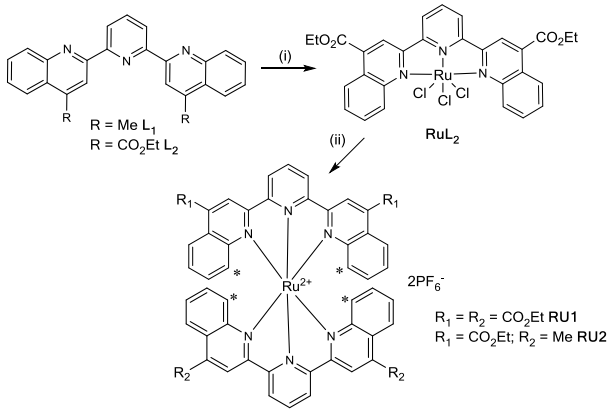

Scheme 1: Reagents and Conditions: (i) $RuCl_3$, EtOH, reflux, $\mathbf{L_2}$ (ii) $AgBF_4$, acetone, *n*-BuOH, reflux, $\mathbf{L_1}$ or $\mathbf{L_2}$. Note: each asterisk marks the 8-hydrogen atom on a quinoline.

The identity of the final complexes was confirmed by ^1H and ^{13}C NMR spectroscopy as well as mass spectrometry. Given that clean NMR spectroscopic data could be collected it is safe to assume that the complexes are diamagnetic and each contains a low-spin d^6 (Ru^{2+}) ion. It was possible to obtain very small but good quality single crystals for the nitrate salt of **RU1**, collect synchrotron X-ray diffraction data, and solve the structure (Figure 2). Selected bond lengths and angles are collected in Table 1. The first point to note is that only two counter-ions are evident and so the oxidation state of the ruthenium is again confirmed to be +2. From inspection of the bond angles it is evident that the metal ion coordination is best described as a distorted octahedron. The N5–Ru–N2 bond angle is close to the ideal 180°, but the other two *trans* bond angles are *ca.* 24° away from this value. As observed in previous $[Ru(terpy)_2]^{2+}$ structures the Ru–N bond lengths to the central pyridine are shorter than the other two Ru–N bond lengths.[13] A major contribution to distortion of the structure is caused by the presence of quinoline rings in the each of the ligands. The 8-hydrogen atom for both quinolines points toward the central pyridine of the complementary ligand. The four hydrogen-to-pyridine centroid distances are between 2.49 Å and 2.79 Å (see Supporting Information). The outcome is a severe twist to the ligand, which is best viewed as two planes created using each quinoline ring (see Supporting Information). The degree of twist for each ligand is somewhat different (32.3° and 12.7°). An additional contribution to distortion for the structure is likely triggered by packing effects, since there is a clear π-stacking motif in the unit cell (see Supporting Information): two quinoline groups for adjacent cations are aligned in a "slipped" parallel configuration at a centroid-to-centroid distance of 3.72 Å. An additional packing effect is seen for one of the ester groups. Near co-planarity of a carbonyl and aryl is expected because of the beneficial increase in π-conjugation. Whereas torsion angles for three of the esters are modest (13.1°, 16.1° and 24.4°) the final angle of 48.9° certainly suggests decoupling of the two groups and there must be a loss in stabilization energy. The reason for this difference is not obvious from the crystal packing diagram (see Supporting Information). As discussed later for computer-calculated structures the result is an anomaly.

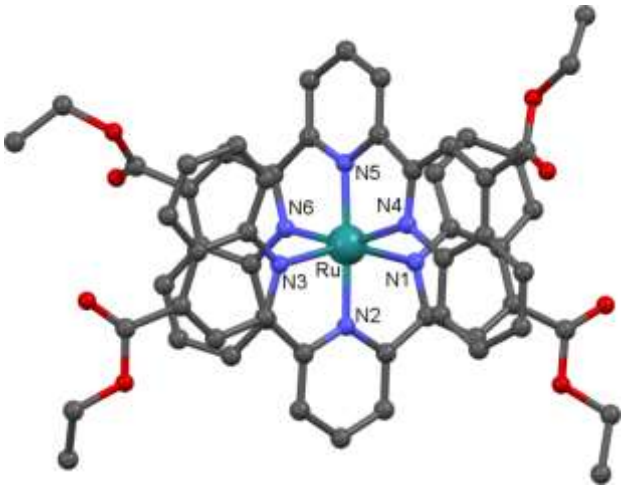

Figure 2. Structure of the cation of **RU1**. H atoms, solvent molecules and nitrate anions are omitted for clarity.

Table 1. Selected bond lengths and angles in the crystal structure of **RU1**.

	Bond Length / Å[a]		Bond Length / Å[a]
Ru–N1	2.150(2) (2.158)	Ru–N4	2.162(2) (2.163)
Ru–N2	1.986(2) (2.006)	Ru–N5	1.989(2) (2.007)
Ru–N3	2.151(2) (2.161)	Ru–N6	2.151(2) (2.162)
	Bond Angle / °		Bond Angle / °
N5–Ru–N2	177.38(9) (179.75)	N6–Ru–N4	156.11(9) (155.52)
N3–Ru–N1	155.69(9) (155.59)		

[a] DFT calculated value using B3PW91 and a 3.21G** basis set is given in parentheses below the crystallographically determined value.

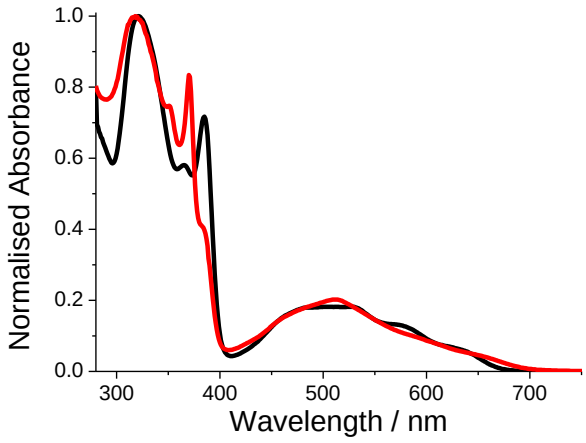

Figure 3. Room-temperature normalised absorption spectra for **RU1** (black) and **RU2** (red) in MeCN.

Absorption/Emission Spectroscopy

The electronic absorption spectra for the two ligands $\mathbf{L_1}$ and $\mathbf{L_2}$ display typically intense bands below 400 nm and are associated with π–π* transitions (see Supporting Information). The two ester groups attached to $\mathbf{L_2}$ help push the absorption envelope toward slightly lower energy, and the overall band shape is broader and has less defined peaks compared to $\mathbf{L_1}$. It is conceivable that n–π* transitions may contribute to the absorption profile for $\mathbf{L_2}$. The absorption spectra collected from dilute MeCN solutions when the ligands are complexed in **RU1** and **RU2** are shown in Figure 3. Besides the ligand-based absorptions below 400 nm, the characteristic metal-to-ligand charge-transfer (MLCT) bands are observed up to around 700 nm. The broad feature for **RU1** actually comprises four peaks at 621 nm, 566 nm, 525 nm and 483 nm. There is compelling evidence to suggest that the multiple band feature is partly a result of interchromophore coupling.[14] Even though **RU1** does not exhibit pure O_h symmetry there is definite loss of symmetry in moving to the heteroleptic complex **RU2**. In addition, the electron affinity of the two ligands is different and, as a consequence, several MLCT states slightly different in energy are feasible. These two factors contribute to the alteration in appearance of the MLCT profile for **RU2**. The main peak is observed at 512 nm and the shoulders either side are less discernible. In solution at room temperature no emission from either **RU1** or **RU2** was observed. Certainly this observation is consistent with previous work on similar derivatives and is explained by the efficient thermally activated non-radiative route via the e_g* orbitals. Time-resolved pump-probe experiments (see Supporting Information) confirmed that the excited state lifetime for **RU1** in MeCN is only 144 ps.

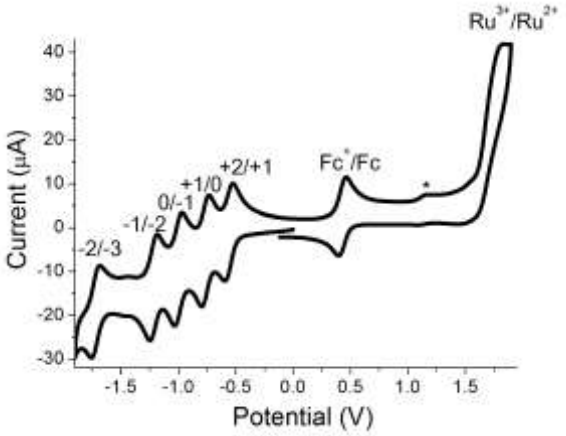

Figure 4. Cyclic voltammogram for **RU1** in MeCN containing 0.1 M TBATFB background electrolyte at a glassy carbon working electrode. Scan rate = 50 mV s^{-1}. * = artefact possibly from deposition of material on the electrode.

Electrochemistry

Prior work by Campagna *et al*.[8] reported the electrochemical behavior of ruthenium(II) complexes of 2,6-bis(4′-phenyl-2′-quinolyl)pyridine. Although up to four ligand-based reductions were reported we found that an additional wave may have been previously overlooked. Cyclic voltammograms were recorded from MeCN solution using 0.1 M *N*-tetrabutylammonium tetrafluoroborate (TBATFB) background electrolyte. The cyclic voltammogram for **RU1** is shown in Figure 4 and data are collected in Table 2. Upon scanning to positive potentials a clear quasi-reversible wave is observed at +1.28 V vs Fc^+/Fc and is readily assigned to redox at the ruthenium center. The scan within the negative potential window is far more detailed and consists of five one-electron reversible waves; observation of the first four waves is in agreement with previous findings.[8] It was not possible to push the scan any further negative because of solvent cut-off. The differences in the half-wave potentials E_2–E_1, E_3–E_2 and E_4–E_3 are very similar (average = 220 mV), but there is a large increase in the difference for the final two couples (E_5–E_4 = 500 mV). The consistency observed in the first three energy gaps is an outcome of the two ligands being identical for **RU1**. The addition of the fifth electron must be to a species that formally has a –2 charge, and the large final energy gap is a

result of the electrostatic penalty. The first four reduction waves can be assigned to sequential addition of an electron to the two ligands.

The cyclic voltammogram for **RU2** (see Supporting Information) contains overall the same basic features as those seen in Figure 4: ruthenium-based redox and five one-electron reductions. The most prominent disparity is observed for the five reduction waves, which appear closer together. The differences in the half-wave potentials E_2–E_1, E_3–E_2, E_4–E_3 and E_5–E_4 are 280, 370, 390 and 270 mV; the effect is a result of the complex containing two dissimilar ligands and the difference in their electron affinic nature. At first it may appear that addition of the fifth electron does not encounter as large an electrostatic penalty when compared to complex **RU1**. However, it is clear that sequential electron additions to **RU2**, at least up to four electrons, become progressively more difficult, as illustrated by the steady increase in ΔE as highlighted in Table 2. The final reduction is still some 210 mV more cathodic for **RU2** when compared to **RU1**. A couple of points are worth noting; namely, the more easily oxidized complex at the ruthenium center is **RU2** and the more easily reduced complex at the ligand centers is **RU1**. Clearly, the main conundrum is this: to which part of the complex does the fifth electron go, considering that after addition of four electrons each ligand would be formally a dianion? The electrochemistry of the "free" ligands was extremely poor, affording no real insight into what may occur in the complexes. Our attention turned to calculations to try to shed light on the problem.

Table 2. Redox potentials measured for the two complexes in dry MeCN and referenced to ferrocene.[a]

Complex	E_1[b] / V +2/+1	E_2[b] /V +1/0	E_3[b]/ V 0/–1	E_4[b] /V –1/–2	E_5[b]/ V –2/–3	E_6[b]/ V Ru^{3+}/Ru^{2+}
RU1	–1.00 (70)	–1.21 (70)	–1.44 (70)	–1.66 (70)	–2.16 (70)	1.28 (130)
RU2	–1.06 (70)	–1.34 (70)	–1.71 (70)	–2.10 (70)	–2.37 (70)	1.10 (90)
ΔE[c] / mV	60 (80)[d]	130	270	440	210	180 (110)[d]

[a] Peak separation E_{pa}–E_{pc} measured to be 70 mV for the ferrocene couple. [b] Half-wave potential ($E_{1/2}$) and peak separation (E_{pa}–E_{pc}) in parentheses. [c] Modulus of the difference between the half-wave potentials **RU2**–**RU1**. [d] Value calculated from DFT results.

Computer Calculations

As a starting point we focused on the two ligands, $\mathbf{L_1}$ and $\mathbf{L_2}$, and in particular mapping electron density distributions as electrons were added sequentially. DFT calculations were performed for the gas phase using the B3LYP correlation function and 6-311G basis set with Gaussian03.[15] The electron density maps shown in Figure 5 help to illustrate in which parts of the ligands electrons may reside after their addition. The starting density distributions for both neutral ligands are in agreement with the electron-donating (methyl group) and -withdrawing (carboxylic ester) effects. The addition of one electron to $\mathbf{L_1}$ places negative density on the central pyridine group, thus avoiding build-up of charge on the quinolone subunits. Addition of two more electrons leads to severe charge accumulation focused on the pyridine. One-electron addition to $\mathbf{L_2}$ does not result in localization of negative charge on any specific aromatic ring. Even after three-electron reduction the negative charge is evenly distributed on the ligand backbone. In view of the calculations it would appear that tri-anion formation, as may be required in the complex, is more favorable for $\mathbf{L_2}$.

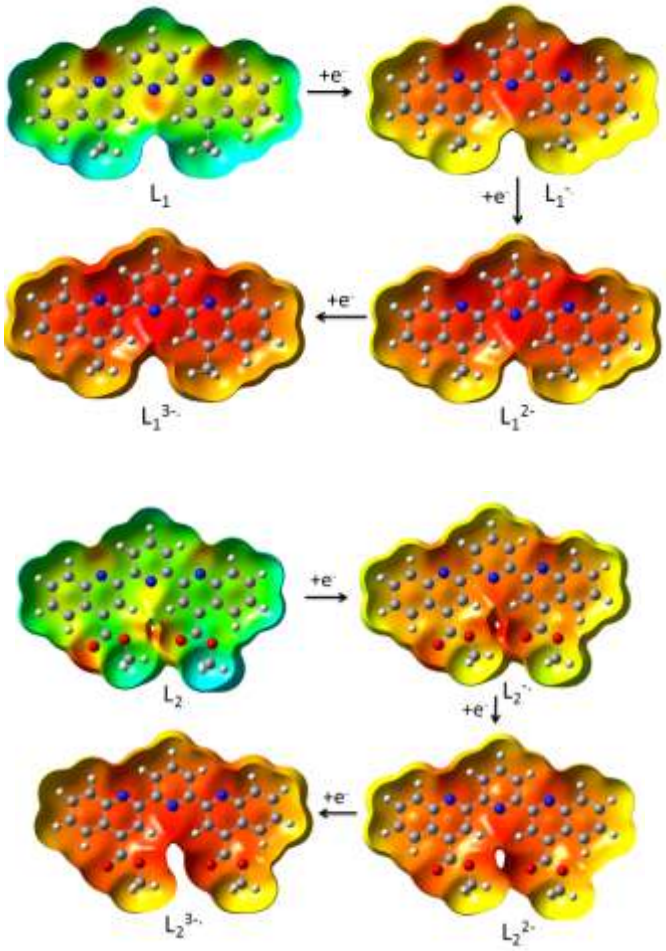

Figure 5. Electron density maps created for the two ligands using Gaussian 03 (B3LYP) and a 6-311G basis set. Blue = low electron density, red = high electron density. Note: to simplify the calculations the methyl ester was used.

Detailed calculations on the ground-state structures for ruthenium(II) complexes of 6-bis(quinolin-2-yl)pyridine type ligands are limited. For example, Onozawa-Komatsuzaki and co-workers[16] reported frontier molecular orbitals for a ruthenium(II) tris-thiocyanato complex using a ZINDO/1 semi-empirical method. Our interest was firstly to construct a comprehensive picture of the LUMO orbitals and use the results to try to explain the electrochemical findings. In the first iteration the ground-state gas phase structures for **RU1** and **RU2** were modeled using the semi-empirical AM1 method. The structures were refined further by DFT using the Perdew non-local correlation

function (B3PW91) and a 3-21G** basis set. Confidence that this method works well is evident by comparison of calculated Ru–N bond lengths with those obtained by X-ray crystallography for **RU1** (Table 1). The poorest correlation is observed for the Ru–N2 and Ru–N5 bond lengths but the difference is less than 1% and within the standard uncertainty of the crystallographically determined value. The computer-calculated and observed bond angles are again in somewhat good agreement. Calculated structures for both **RU1** and **RU2** are collected in the Supporting Information along with models displaying the "twist" angles for the two ligands; values appear reasonable and are around 29° (cf. 12.6° and 32.3° for **RU1**). Recalling that at least one torsion angle for the carbonyl group within **RU1** is likely distorted by packing effects, the average torsion angle from calculated structures is only 0.9°.

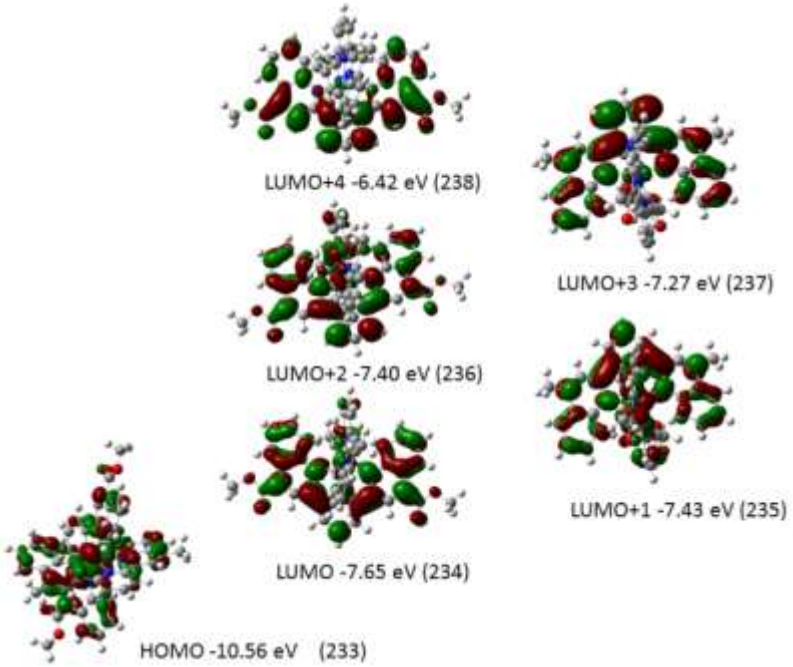

Figure 6. DFT calculated (B3PW91, 3.21G**) selected frontier molecular orbitals for **RU2**. The number of the molecular orbital is given in parentheses.

A selection of DFT calculated frontier molecular orbitals for the heteroleptic complex **RU2** are collected in Figure 6. For a low-spin Ru^{2+} (d^6) metal ion in an octahedral field simple crystal field theory predicts the HOMO must be based on the t_{2g} set of orbitals (d_{xy}, d_{xz}, d_{yz}).[17] Since for **RU2** the coordination sphere is distorted the pure degeneracy of the t_{2g} orbitals is removed and, as shown in Figure 6, the HOMO (233) mainly comprises the d_{xy} orbital. The LUMO (234) is localized on $\mathbf{L_2}$, which incorporates the two electron-withdrawing ester groups and is quinoline-based. In contrast the LUMO+1 (235) is sited on $\mathbf{L_1}$ but is more biased towards the central pyridine ring. Very close in energy is the LUMO+2 (236) and it is shifted back to reside on $\mathbf{L_2}$. This flipping of spatial location is again observed in moving from LUMO+2 to LUMO+3 (237) and finally LUMO+4 (238), but there is a considerable energy difference (0.85 eV) between these last two orbitals. In contrast, it is noted that the difference in energy from LUMO to LUMO+3 is rather modest (0.38 eV). Calculations were also performed on the singly and doubly reduced forms of **RU2** to assess if reduction perturbed the structure to any major extent.[18] We could map any modifications to spatial distributions of the frontier molecular orbitals (see Supporting Information). The sequential addition of an electron to **RU2** results as expected in a shortening of the Ru–N bonds as electron density is increased on the ligands. There are small modifications to the N–Ru–N bond angles to accommodate the bond length changes. In addition the "twist" of the two ligands is slightly exaggerated as the angles are increased. If we ignore the anticipated change in orbital energies, the frontier molecular orbitals from 235 to 237 remain relatively close in energy and there is still a significant energy gap between orbitals 237 and 238.

Results of similar ground-state molecular orbital calculations performed on **RU1** are collected in the Supporting Information. Overall, the findings are similar, although it is noticed that the HOMO and LUMO for **RU1** are lower in energy compared to analogous orbitals for **RU2**. Consequently, the calculations predict that the ruthenium(II) center for **RU2** will be the easier to oxidize of the two complexes (ΔE = 110 mV). In contrast, ligand-based reductions for **RU1** will be slightly more facile (ΔE = 80 mV). The two predictions turn out to be remarkably good. Again the good agreement between theory and experiment does suggest that the DFT calculation method is reliable.

Although calculations could not definitively answer the conundrum of the exact location of the fifth electron, the ligand $\mathbf{L_2}$ in the complex is the more likely site. The electron-withdrawing ester groups help stabilize any electron density build up on the ligand and seem to facilitate the spreading out of negative charge.

Conclusions

Despite the poor photochemistry of ruthenium(II) complexes bearing bis(quinolin-2-yl)pyridine ligands, their electrochemistry is more rewarding than initially described. Complexes bearing the electron-withdrawing ester-functionalized ligand are capable of storing reversibly five electrons. The electron storage capacity may be even greater by further modification of the ligand skeleton. Highly electron-withdrawing groups (e.g., CN, CF_3) could facilitate storage to six or even seven electrons by stabilization of the highly charged ligands. Considering the focus of C_{60} and its multiple-electrons storage capability[19] the metal-based complexes described here may open up new avenues for reversible charge storage.

Experimental Section

All experiments were performed under a nitrogen atmosphere. All solvents, deuterated solvents and starting reagents were purchased from Sigma Aldrich and Alfa Aesar, and were used as received. NMR spectra were recorded on Bruker 300, JEOL 400 or Bruker Ultrashield 400 plus spectrometers. FT-IR spectra were recorded on a Varian 800FT-IR or a Perkin Elmer Spectrum 100 FT-IR spectrophotometer. MS analyses were performed by the EPSRC National Mass Spectrometry Service Centre, College of Medicine, Swansea University. Ultraviolet–visible (UV–vis) absorption spectra were measured with a Perkin Elmer Lambda 25 spectrometer. Voltammetry studies were carried out using a CH Instruments electrochemical analyzer. Acetonitrile was distilled over CaH_2; $TBABF_4$ (Sigma Aldrich) was used without further purification. Dinitrogen presaturated with MeCN flowed into the cell before voltammetric experiments. Computational calculations were performed using a 32-bit version of Gaussian03 on a quadruple-core Intel Xeon system with 4GB RAM. The calculations were run in parallel, fully utilizing the multi-core processor. Energy minimization calculations were monitored using Molden and run in parallel with frequency calculations to ensure that optimized geometries represented local minima. Calculations performed on reduced species for both ligands and complexes were run at the singlet and doublet levels only.

Preparation of 2,6-bis(4-methylquinolin-2-yl)pyridine (L_1)

In a small round-bottom flask was placed a saturated solution of C_2H_5OK in EtOH (3 mL). After cooling to 0° C, 2,6-diacetylpyridine (0.344 g, 2.63 mmol) was added and the mixture was stirred until the solution turned yellow. When all the 2,6-diacetylpyridine had dissolved, 2-aminoacetophenone (0.71g, 5.26 mmol) was added dropwise and the mixture was stirred for 2 h at 5° C. After 20 h of stirring at room temperature a white precipitate formed, which was collected by filtration, washed with EtOH and recrystallized from THF to give colorless crystals of **L_1** (0.571g, 60%.). IR (cm^{-1}): 3065 (w), 2972 (w), 1596 (s), 1554 (s), 1508 (s), 1442 (s), 1347 (s), 1256 (w), 1197 (m), 1141 (m), 1032 (m), 993 (m), 886 (m), 827 (s), 736 (vs), 673(s). ^{1}H NMR (300 MHz, $CDCl_3$) δ 8.74 (d, 2H, *J* = 7.8 Hz), 8.66 (s, 2H), 8.21 (d, 2H, *J* = 8.3 Hz), 8.10–8.00 (m, 3H), 7.75 (td, 2H, *J* =1.2, 7.0 Hz), 7.59 (td, 2H, *J* =1.0, 7.0 Hz), 2.88 (s, 6H). ^{13}C NMR (75 MHz, $CDCl_3$) δ 156.17, 148.31, 144.87, 138.59, 137.86, 130.82, 129.31, 128.66, 126.65, 123.89, 122.30, 119.87, 19.12. FTMS $[M+H]^+$ calculated for $C_{25}H_{20}N_4$ (found): 362.1651 (362.1652). λ_{max} ($CHCl_3$) = 325 nm.

Preparation of 2,6-bis(4-carboxyquinolin-2-yl)pyridine, sodium salt (1)

In a 100 ml round-bottom flask were thoroughly mixed solid isatin (1g, 6.75mmol) and 2,6-diacetylpyridine (0.55g, 3.375 mmol). The flask was immersed in an ice bath, and an ice-cold solution of 33% NaOH (3.75 g) was added with stirring. Stirring and warming was continued until the contents hardened (at this point the temperature was approximately 60° C). Ice water (4 mL) was then added to produce a fine purple/red slurry (with a metallic sheen). The suspension was cooled to 5° C and filtered, giving a purple/red solid crude product. The solid was washed with water (1 mL), and the colored impurities were removed by generous washing with acetone. The solid was allowed to dry, and was recrystallized from a minimum amount of hot water. Activated carbon was added to remove the remaining colored impurities. The crystallization was repeated, until no colored impurities remained, to afford **1** as colorless plates (0.544 g, 34 %). M.p. >300 °C. IR (cm^{-1}): 3260 (w), 1602 (s), 1572 (s), 1549 (s), 1506 (m), 1428 (s), 1388 (vs), 1339 (s), 1251 (m), 1150 (m), 1090 (w), 1025 (w), 994 (w), 870 (w), 811 (m), 772 (s), 763 (s), 693(w), 666 (w).

Preparation of 2,2′-(pyridine-2,6-diyl)diquinoline-4-carboxylic acid (2)

The sodium salt **1** (0.5 g, 1.19 mmol) was dissolved in water (30 ml). The solution was neutralized with 10% HCl solution. The acid **2** is soluble in acidic solution, and care should be taken not to over-acidify; a pH of 7 is optimum. The free acid **2** is a colorless high melting point solid, and samples obtained at lower pH contain a yellow cast, probably due to the presence of the HCl salt. The solid was filtered, washed with water (3 × 10 mL) and air-dried, giving **2** as a light yellow solid (0.44 g, 97 %). M. p. > 300° C. IR (cm^{-1}): 3447 (w), 1696 (vs), 1588 (m), 1563 (w), 1553 (m), 1506 (w), 1463 (w), 1415 (m), 1343 (m), 1278 (s), 1238 (s), 1151 (w), 1087 (m), 922 (m), 830 (m), 797 (m), 767 (vs), 737 (s), 669 (w), 686 (m). ^{1}H NMR (400 MHz, d_6-DMSO) δ 9.15 (s, 2H), 8.77 (dd, *J* = 7.8 Hz, 3.8 Hz, 4H), 8.29 (t, *J* = 7.8 Hz, 1H), 8.25 (d, *J* = 7.9 Hz, 2H), 7.91 (td, *J* = 1.3, 8.3 Hz, 2H), 7.78 (td, *J* = 1.3, 7.7 Hz, 2H). ^{13}C NMR (101 MHz, d_6-DMSO) δ 168.09, 155.28, 154.81, 148.67, 139.48, 138.02, 130.88, 130.48, 129.06, 126.13, 125.08, 122.77, 119.58, 31.17; λ_{max} (DMF) = 315 nm.

Preparation of diethyl 2,2′-(pyridine-2,6-diyl)diquinoline-4-carboxylate (L_2)

In a round-bottom flask conc. H_2SO_4 (90 mL) was added carefully with vigorous stirring to EtOH (180 ml). After a few minutes of stirring **2** (0.884g, 2.1 mmol) was added and after 20 h of refluxing the transparent solution was cooled to room temperature and diluted with 300 mL of ice. The reaction mixture was neutralized with NaOH (25%) solution to pH 8. The yellow precipitate was filtered off, washed with water (3 × 75 mL) and EtOH (10 mL) and air-dried to give **L_2** (0.90 g, 90 %). IR (cm^{-1}): 3058 (w), 2982 (w), 2905 (w), 1736 (s), 1714 (s), 1587 (m), 1555 (m), 1508 (w), 1465 (w), 1451 (w), 1396 (w), 1374 (m), 1342 (w), 1260 (s), 1228 (vs), 1185 (s), 1152 (s), 1092 (m), 1036 (s), 1022 (s), 996 (m), 921 (w), 907 (w), 871 (w), 825 (m), 795 (m), 771 (s), 736 (m), 695 (w), 668 (w). ^{1}H NMR (400 MHz, $CDCl_3$) δ 9.29 (s, 2H), 8.78 (d, *J* = 7.8 Hz, 2H), 8.77 (d, *J* = 8.5 Hz, 2H), 8.27 (d, *J* = 8.4 Hz, 2H), 8.10 (t, *J* = 7.8 Hz, 1H), 7.81 (td, *J* =1.2, 7.6 Hz , 2H), 7.68 (td, *J* =1.2, 7.7 Hz, 2H), 4.59 (q, *J* = 7.1 Hz, 4H), 1.56 (t, *J* = 7.1 Hz, 6H). ^{13}C NMR (101 MHz, $CDCl_3$) δ 166.79, 155.75, 155.08, 149.14, 138.09, 136.64, 130.61, 129.96, 128.40, 125.75, 125.09, 122.48, 120.46, 61.99, 14.39. FTMS $[M+H]^+$ calculated for $C_{29}H_{24}N_3O_4$ (found): 478.1749 (478.1761). λ_{max} ($CHCl_3$) = 312, 322 nm.

Preparation of RuL_2

To absolute ethanol (30 mL) in a 100 ml round-bottom flask were added $RuCl_3 \cdot xH_2O$ (0.11 g (0.42 mmol) and **L_2** (0.2 g, 0.42 mmol) under N_2. The mixture was heated at reflux for 20 h in the dark. After this time the reaction mixture was concentrated under vacuum and the green powder was filtered from the solution. The product was washed with EtOH (3 × 15 mL) and Et_2O, until the filtrate became transparent. The solid was air-dried to give the product **RuL_2** (0.226 g, 79 %). IR (cm^{-1}): 3069 (w), 2997 (w), 1715 (vs), 1524 (s), 1476 (m), 1431 (m), 1372 (s), 1328 (m), 1255 (vs), 1231 (vs), 1198 (vs), 1152 (s), 1120 (s), 1027 (vs), 952 (w), 905 (w), 859 (m), 767 (vs), 675 (m), 630 (m).

Preparation of RU1

To a green suspension of **RuL_2** (0.226 g, 0.316 mmol) in acetone (40 mL) was added $AgBF_4$ (0.184g, 0.947 mmol) and the mixture was heated

to reflux for 2 h. The resulting purple suspension was filtered to remove precipitated AgCl. The acetone was removed and the reside was dissolved in *n*-butanol (100 ml); to this was added **L_2** (0.151 g, 0.316 mmol). The solution was refluxed under N_2 in the dark for 24 h. After cooling, the solvent was evaporated and the residue was dissolved in CH_3OH (100 mL), and excess KPF_6 (0.5 g) in water (50 mL) was added. The red precipitate was collected by filtration, washed with water and air-dried. The crude product (0.450 g) was redissolved in the minimum volume of CH_3CN for column chromatography over silica, using CH_3CN, water, and saturated aqueous KNO_3 (10:1:0.5) as eluent. The pure complex after chromatography was dissolved in CH_3OH and excess KPF_6 solution was added. The dark purple precipitate was collected, dried and recrystallized from a minimum amount of CH_3CN/toluene to afford dark purple crystals (0.224 g, 53%). IR (cm^{-1}): 3077 (w), 2919 (w), 1721 (vs), 1594 (w), 1536 (s), 1326 (s), 1261 (vs), 1204 (vs), 1151 (s), 1026 (vs), 910 (w), 861 (m), 824 (m), 773 (vs), 621 (m). ^{1}H NMR (300 MHz, $CDCl_3$+CD_3OD) δ 9.33 (d, *J* = 8.2 Hz, 4H), 8.91 (t, *J* = 8.2 Hz, 2H), 8.76 (s, 4H), 8.44 (d, *J* = 8.6 Hz, 4H), 7.49 (t, *J* = 7.6 Hz, 4H), 7.23 (t, *J* = 7.6 Hz, 4H), 6.42 (d, *J* = 8.6 Hz, 4H), 4.38 (q, *J* = 7.1 Hz, 8H), 1.33 (t, *J* = 7.1 Hz, 12H). FTMS $[M-H]^+$ calculated for **RU1**·$2H_2O$ $C_{58}H_{50}N_6O_{10}Ru$ (found) 1091.2096 (1092.1218).

Preparation of RU2

To a green suspension of **RuL_2** (0.173 g, 0.242 mmol) in acetone (40 mL) was added $AgBF_4$ (0.141g, 0.726 mmol) and the mixture was heated to reflux for 2 h. The resulting purple suspension was filtered to remove precipitated AgCl and was washed with acetone. Once the acetone was removed, *n*-butanol (100 ml) and **L_1** (0.087 g, 0.24 mmol) were added, and the solution was refluxed under N_2 in the dark for 12 h. The solvent was evaporated and the residue was dissolved in acetonitrile. After anion exchange purification of the crude product (0.23 g) the product was purified by column chromatography on silica gel using CH_3CN/water/saturated aqueous KNO_3 mixture (10:2:1) as eluent. After anion exchange the dark purple precipitate was collected, dried, and recrystallized from a minimum amount of CH_3CN/toluene to afford dark purple crystals (0.1 g, 34 %). IR (cm^{-1}): 3097 (w), 1723 (vs), 1597 (s), 1536 (s), 1436 (m), 1372 (s), 1263 (s), 1209 (m), 1153 (m), 1124 (m), 1028 (m), 835 (vs), 773 (s), 669 (m), 622 (m). ^{1}H NMR (400 MHz, CD_3CN) δ 9.21 (d, *J* = 8.2 Hz, 2H), 9.08 (d, *J* = 8.2 Hz, 2H), 8.82 (t, *J* = 8.6 Hz, 2H), 8.68 (s, 2H), 8.43 (d, *J* = 8.6 Hz, 2H), 8.30 (s, 2H), 7.90 (d, *J* = 8.4 Hz, 2H), 7.60 (td, *J* = 1.1, 8.2 Hz, 2H), 7.53 (td, *J* = 1.1, 8.2 Hz, 2H), 7.28 (td, *J* = 1.5, 8.6 Hz, 2H), 7.21 (td, *J* = 1.4, 8.6 Hz, 2H), 6.62 (d, *J* = 8.5 Hz, 2H), 6.41 (d, *J* = 8.4 Hz, 2H), 4.45 (q, *J* = 7.1 Hz, 4H), 2.71 (s, 6H), 1.40 (t, *J* = 7.1 Hz, 6H). ^{13}C NMR (101 MHz, CD_3CN) δ 190.61, 165.17, 161.03, 160.39, 159.49, 159.35, 151.49, 149.55, 139.75, 132.90, 132.58, 131.12, 130.10, 129.67, 127.71, 126.96, 125.33, 121.78, 120.72, 63.83, 49.81, 18.91. FTMS $[M-PF_6]^+$ calculated for $C_{54}H_{42}F_6N_6O_4PRu$ (found) 1085.1952 (1084.9838).

X-ray crystallography

Data for **L_1** and **L_2** were measured on Agilent Technologies diffractometers with Mo$K\alpha$ radiation, while the very small crystals of **RU1** were examined with synchrotron radiation at beamline I19 of Diamond Light Source. Full details are given in the Supporting Information. CCDC reference numbers: 1033746–1033748.

Acknowledgements

This work was funded by the FP7-PEOPLE-2009-IRSES Nr. 246902 grant and Newcastle University. The Engineering and Physical Sciences Research Council (EPSRC) National Mass Spectrometry Service at Swansea is thanked for collecting mass spectra; EPSRC is also thanked for equipment grant EP/F03637X/1. Diamond Light Source is thanked for access to beamline I19 for diffraction data for **RU1**.

Keywords: ruthenium, complex, polypyridine, electrochemistry, X-ray crystallography, DFT calculations

[1] a) M. H. V. Huynh, D. M. Dattelbaum, T. J. Meyer, *Coord. Chem. Rev.* **2005**, *249*, 457-483; b) J.-P. Sauvage, J.-P. Collin, J.-C. Chambron, S. Guillerez, C. Coudret, V. Balzani, F. Barigelletti, L. De Cola, L. Flamigni, *Chem. Rev.* **1994**, *94*, 993-1019; c) E. Baranoff, J.-P. Collin, L. Flamigni, J.-P. Sauvage, *Chem. Soc. Rev.* **2004**, *33*, 147-155.

[2] H, Hofmeier, U. S. Schubert, *Chem. Soc. Rev.* **2004**, *33*, 373-399; b) E. C. Constable, *Chem. Soc. Rev.* **2007**, *36*, 246-253.

[3] A. C. Benniston, *Chem. Soc. Rev.* **2004**, *33*, 573-578.

[4] E. A. Medlycott, G. S. Hanan, *Chem. Soc. Rev.* **2005**, 34, 133-142

[5] A. Amini, A. Harriman, A. Mayeux, *Phys. Chem. Chem. Phys.* **2004**, *6*, 1157-1164.

[6] M. L. Stone, G. A. Crosby, *Chem. Phys. Lett.* **1981**, *79*, 169-173.

[7] M. Abrahamsson, M. Jäger, T. Österman, L. Eriksson, P. Persson, H-C. Becker, O. Johansson, L. Hammarström, *J. Am. Chem. Soc.* **2006**, 128, 12616-12617.

[8] S. Campagna, A. Mamo, J. K. Stille, *J. Chem. Soc., Dalton Trans.* **1991**, 2545-2551.

[9] Q. Li, S. Surthi, G. Mathur, S. Gowda, Q. Zhaom T. A. Sorenson, R. C. Tenent, K. Muthukumaran, J. S. Lindsey, V. Misra, *App. Phys. Lett.* **2004**, *85*, 1829-1831.

[10] B. Fabre, *Acc. Chem. Rev.* **2010**, *43*, 1509-1518.

[11] For examples of other work looking at complexes that are multiply reduced see: M. Wang, J. England, T. Weyhermüller, K. Weighardt, *Inorg. Chem.* **2014**, 53, 2276-2287. A. C. Bowman, J. England, S. Sproules, T. Weyhermüller, K. Weighardt, *Inorg, Chem.* **2013**, 52, 2242-2256. C. C. Scarborough, K. M. Lancaster, S. DeBeer, T. Weyhermüller, S. Sproules, K. Weighardt, *Inorg. Chem.* **2012**, 51, 3718-3732. A. Paretzki, M. Bubrin, J. Fielder, S. Záliš, W. Kaim, *Chem. Eur. J.* **2014**, 20, 5414-5422. A. K. Das, R. Hübner, B. Sarkar, J. Fiedler, S. Záliš, G. K. Lahiric, W. Kaim, *Dalton Trans.* **2012**, 41, 8913-8921.

[12] J. A. Knight Jr, H. K. Porter, P. K. Calaway, *J. Am. Chem. Soc.* **1944**, *66*, 1893-1894.

[13] E. C. Constable, C. E. Housecroft, M. Neuburger, D. Phillips, P. R. Raithby, E. Schofield, E. Sparr, D. A. Tocher, M. Zhender, Y. Zimmermann, *J. Chem. Soc., Dalton Trans.* **2000**, 2219–2228.

[14] a) M. L. Myrick, R. L. Blakley, M. K. De Armond, *J. Phys. Chem.* **1989**, *93*, 3936-3940 ; b) M. L. Myrick, M. K. De Armond, R. L. Blakley, *Inorg. Chem.* **1989**, *28*, 4077-4084.

[15] M. J. Frisch, G. W. Trucks, H. B. Schlegel, G. E. Scuseria, M. A. Robb, J. R. Cheeseman, J. A. Montgomery, Jr., T. Vreven, K. N. Kudin, J. C. Burant, J. M. Millam, S. S. Iyengar, J. Tomasi, V. Barone, B. Mennucci, M. Cossi, G. Scalmani, N. Rega, G. A. Petersson, H. Nakatsuji, M. Hada, M. Ehara, K. Toyota, R. Fukuda, J. Hasegawa, M. Ishida, T. Nakajima, Y. Honda, O. Kitao, H. Nakai, M. Klene, X. Li, J. E. Knox, H. P. Hratchian, J. B. Cross, V. Bakken, C. Adamo, J. Jaramillo, R. Gomperts, R. E. Stratmann, O. Yazyev, A. J. Austin, R. Cammi, C. Pomelli, J. W. Ochterski, P. Y. Ayala, K. Morokuma, G. A. Voth, P. Salvador, J. J. Dannenberg, V. G. Zakrzewski, S. Dapprich, A. D. Daniels, M. C. Strain, O. Farkas, D. K. Malick, A. D. Rabuck, K. Raghavachari, J. B. Foresman, J. V. Ortiz, Q. Cui, A. G. Baboul, S. Clifford, J. Cioslowski, B. B. Stefanov, G. Liu, A. Liashenko, P. Piskorz, I. Komaromi, R. L. Martin, D. J. Fox, T. Keith, M. A. Al-Laham, C. Y. Peng, A. Nanayakkara, M. Challacombe, P. M. W. Gill, B. Johnson, W.

Chen, M. W. Wong, C. Gonzalez, and J. A. Pople, Gaussian, Inc., Wallingford CT, (2004).
[16] N. Onozawa-Komatsuzaki, M. Yanagida, T. Funaki, K. Kasuga, K. Sayama, H. Sugihara, *Inorg. Chem. Commun.* **2009**, *12*, 1212-1215.
[17] J.-P. Launay, M. Verdaguer, Electrons in Molecules: From Basic Principles to Molecular Electronics, Oxford University Press, **2014**.
[18] DFT calculations were also performed up to the addition of five electrons to the complex. No further insightful information was obtained from the calculations and addition of electrons appeared to be ligand based. It should be noted that there are many deficiencies in using DFT calculations to map orbital analysis to the redox activity. No account is taken of reorganisation energies following electron additions and reordering of orbitals. Calculations were also only performed at the singlet and doublet levels and any heavy atom effect for the complexes was ignored.
[19] J. Chlistunoff, D. Cliffel, A. J. Bard, *Thin Solid Films*, **1995**, 257, 166-184.

The two ligands diethyl 2,2′-(pyridine-2,6-diyl)bis(quinolone-4-carboxylate) (**L_2**) and 2,6-bis(4-methylquinolin-2-yl)pyridine (**L_1**) were used to prepare the homoleptic $[Ru(\mathbf{L_1})_2](PF_6)_2$ (**RU1**) and heteroleptic $[Ru(\mathbf{L_1})(\mathbf{L_2})](PF_6)_2$ (**RU2**) complexes. Electrochemistry experiments showed that the complexes can hold up to five electrons reversibly.

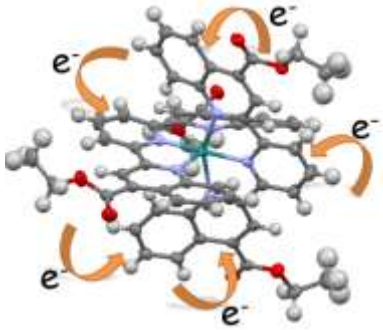

Ion Marin, Constantin Turta, Andrew C. Benniston, Ross W. Harrington, William Clegg*

Page No. – Page No.

Homoleptic and Hetroleptic Ruthenium(II) Complexes based on 2,6-bis(quinoline-2-yl)pyridine Ligands: Multiple Charge State Modules for Potential Density Memory Storage